Primary Calibration of Acoustic Emission Sensors by the Method of Reciprocity, Theoretical and Experimental Considerations

Thomas Monnier, Dia Seydou, Nathalie Godin, Fan Zhang

Primary Calibration of Acoustic Emission Sensors by the Method of Reciprocity, Theoretical and Experimental Considerations

Thomas MONNIER[1], Seydou DIA[2], Nathalie GODIN[2], Fan ZHANG[3]

[1] Université de Lyon, INSA-Lyon, LVA EA 677, F-69621 Villeurbanne
e-mail: thomas.monnier@insa-lyon.fr
[2] Université de Lyon, INSA-Lyon, MATEIS UMR 5510, F-69621 Villeurbanne
[3] CETIM; Senlis, France

Abstract
This paper is focused on the calibration of acoustic emission (AE) sensors by means of the reciprocity method. Therefore, the problem of the reciprocity criterion in the case of ultrasonic waves in solid is addressed. This latter criterion is well established and widely used for the calibration of electro-acoustic transducer. However, and despite that the first papers have been published forty years ago, its application in the case of ultrasonic wave in solids now raises a number of discussions in the community of acoustic emission. To start with, we present a review of the concept of reciprocity since its origin in electromagnetism to its application to electro-acoustic transducers. We follow a critical analysis on the validity of the reciprocity theorem in the case of AE sensors. Next, a new aperture function will be presented, reconsidering the classical assumption of a constant sensitivity of the transducer's sole by achieving an experimental estimation of its actual vibration using contactless laser interferometry. Finally, an original method for shear wave calibration of AE sensors will be presented.

Keywords: Acoustic Emission, AE sensors, Calibration, Reciprocity Method, Aperture Effect.

1. Introduction

The reciprocity method is based upon the reciprocity theorem. In the field of electrical networks the following statement can translate the reciprocity theorem: "a given e.m.f. in the *p-th* branch will produce the same current in the *q-th* branch of a circuit as the same e.m.f. in the *q-th* branch would produce in the *p-th* branch" [1]. As a consequence of the principle of electro-mechanical equivalence, this theorem is applied to ultrasonic transducer.

McLean [2] was the first to propose a reciprocity-based technique for the calibration of electroacoustic transducers. The reciprocity technique has since then been developed and extended to carry out primary calibration of microphones, accelerometers and ultrasonic sonar transducers. It appears that this technique can be developed further to carry out calibration of transducers operating on an isotropic solid medium [3], and in particular for acoustic emission sensors as first proposed formally by Hatano [4].

The basic principle of the reciprocity calibration method is that three transducers, all of which are uncalibrated, are used as emitter and receiver successively. The basic experimental arrangement is shown in Figure 1.

The conditions of validity of this method are defined as follows:

- AE sensors are assumed linear and reversible
- The coupling of the sensors must be reproducible (defined materials, constant thickness) [5]
- The propagation medium is free of interference referred to the wave (attenuation, reflections, conversions, etc.)

As shown in Figure 1, reciprocity calibration process consists of three steps. Each step involves two sensors: the emitter and the receiver. At each step current absorbed by the emitting sensor and voltage across the receiving sensor are measured. The sequence is repeated for the three AE sensors pairs.

Finally, computation performed on the measured voltages and currents yields the sensitivities of all three sensors. The reciprocity calibration process is relatively straightforward. The receiving sensitivity of sensor 2 can be written as:

$$M_2 = \sqrt{\frac{H E_{12} E_{23} I_{31}}{I_{12} I_{23} E_{31}}}$$

where H is the reciprocity parameter. H is frequency dependent and is defined as the ratio M/S for a given transducer. M is the receiving sensitivity of the transducer, and S the emitting sensitivity of the transducer. In this paper we review the theoretical basis of the reciprocity parameter and reciprocity calibration of AE sensors.

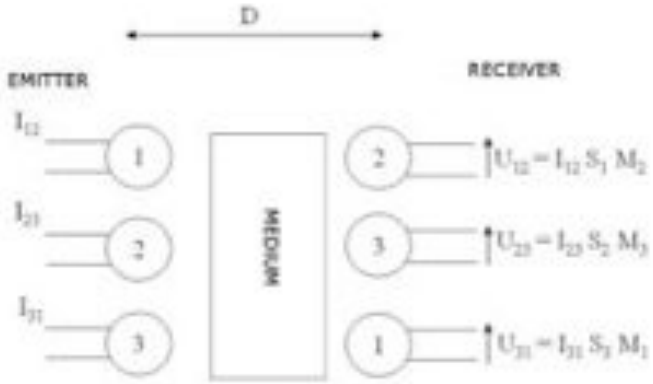

Figure 1: Methodology of reciprocity calibration of AE sensors

Using this methodology, we obtain the reception sensitivity curve of the sensor to be calibrated with a reproducibility on the sensitivity to the resonant frequency of the order of 2dB, with some limitations:

- Only the surface wave response is available in the frequency band of 50 kHz to 1 MHz
- Some difficulties remain to calibrate sensors low frequencies

For what concerns Rayleigh waves calibration, our results are consistent with those obtained by the original work of Hatano [6] and those recently shown by other research teams [7-9]

This article is divided into three parts. The first section discusses the question of reciprocity criterion in the case of AE sensors. Then follows the introduction of a new aperture function. Finally, an original method for shear wave (S-wave) calibration of AE sensors will be presented.

2. The reciprocity parameter

To give a proper definition of the reciprocity parameter is not a simple task. Generally, the reciprocity parameter is defined by either quoting an equation or quoting a definition, neither of which gives any physical insight into the meaning of the parameter. The literature on acoustic reciprocity calibration is also confusing although the measurement procedure is relatively straightforward.

To our knowledge the only theoretical work on the reciprocity method in the case of acoustic transducer is owed to Bobber [10]. He showed that the reciprocity parameter can be expressed as the ratio of acoustic *volume velocity* to the *mean pressure* at the face of the transducer. He also proved that the reciprocity parameter is actually the transfer admittance of

the medium. He deduced from that, reciprocity parameter for: (i) spherical wave, (ii) plane wave, (iii) acoustic couplers, (iv) diffused sound, (v) tubes.

Bobber's conclusions are relevant to the case of transducers totally immersed in fluid medium. Since in standard operation AE sensors are stuck to the external surface of solid medium, how reciprocity parameter can be derived?

Hill and Adams [5] gave the answer to that question, by defining AE measurement procedure in terms of transfer functions. Dimensional analysis of the equations obtained yields that the medium is excited by a *surface velocity*. Hill and Adams noted that this observation is consistent with the transformation of electrical to acoustical quantities. Most of the theories relating to the calibration of ultrasonic transducers in fluid use *volume velocity* for the source output and *acoustic pressure* as the received quantity. However, Hill and Adams have shown that other input and output quantities are possible. Among these possibilities, the ratio *Velocity/Force* is indicated for AE sensors. As a result R-wave reciprocity parameter is obtained from the basic theory of surface wave propagation on a semi-infinite half space – Lamb [11]. Hill and Adams showed that considering a point force driving the surface derives the reciprocity parameter, yielding vertical velocity a distance *d* away. This definition is the starting point for the finite element simulations we conducted in our laboratory. However, the results are not consistent with the conclusions of Hill and Adams. Further investigations are currently conducted. Various expressions of the reciprocity parameter according to the type of wave and the propagation medium are summarized in Table 1, all coming from [12] except for S-ware. In that particular case, we simply propose to adopt the same definition as for L-waves but replacing the expression of longitudinal wave velocity by the shear wave velocity.

Table 1: Expressions of reciprocity parameter

Medium	**Geometrical arrangement**	**Reciprocity Parameter *H***
Fluid	Spherical wave	$\frac{2d}{\rho f}$
	Plane wave	$\frac{2A}{\rho C}$
Solid	Rayleigh wave (R-wave)	$\left[\frac{K2\pi f(1+\sigma)k}{E}\left(\frac{2}{\pi kd}\right)^{1/2}\right]^{-1}$ $k = 2\pi f\left[\frac{2(1+\sigma)\rho}{E}\right]^{1/2} Y$
	Longitudinal wave (L-wave)	$\frac{dE(1-\sigma)}{2f(1+\sigma)(1-2\sigma)}$
	Shear wave (S-wave)	$\frac{dE}{4f(1+\sigma)}$

d is the propagation path distance, ρ is the material density, *f* is the calibration frequency, *C* is the compliance of coupling medium, *K* and *Y* are numerical solutions to Lamb's equation for specific values of Poisson's ratio, σ is the material Poisson's ratio, *E* is Young's modulus.

So far we have pointed the question of the definition of the reciprocity parameter. Now, it is necessary to make some special remarks about the fulfillment of the reciprocity criterion in the case of AE sensors.

The case of bulk waves (e.g. L-wave) is handled in Bobber's paper. In that case the reciprocity criterion is met for AE sensors. In the case of surface wave (R-wave), a phenomenon, called the aperture effect, makes possible the existence of frequencies, at which the sensor response is null. Thus, for these cut-off frequencies, the sensor can emit but cannot hear anything. Consequently reciprocity is not met.

Bobber defined a general reciprocity parameter for electro-acoustical transducer. Hill and Adams have defined the reciprocity parameter for AE sensors calibration. Although AE sensors in L-wave configuration met the reciprocity criterion, it is not the case for R-wave configuration due to aperture effect. In the next section we shall go into more details about the aperture function. First, a classical approach will be used to define it. Next, a new aperture function based on an original approach will be presented.

3. The aperture effect

Let us consider a wave, propagating on the surface of a propagation medium. An AE sensor is positioned on the propagation medium. When the sensor is submitted to the surface wave, the normal vibration velocity at each point of its face is not uniform. It can be derived that the voltage across the sensor is proportional to the average vibration velocity. Such average depends on the wavelength of the incident wave and the sensor diameter. This phenomenon, called the aperture effect, acts as a filter applied to the R-wave sensitivity of the sensor. The complex value of this filter in the frequency domain is called the aperture function. It has been shown that removing the aperture effect by combining the sensor's aperture function with its R-wave sensitivity yields its L-wave sensitivity.

To illustrate this phenomenon, Figure 2 pictures the displaced surface of a sine wave for which the average movements gives zero values for the sensor's response at certain cut-off frequencies. For AE sensor larger than the wavelengths of interest, the classical recommendation to overcome this limitation simply consists in choosing sensing elements with a diameter as small as other constraints allow.

It has been shown [13, 14] that the voltage output of AE transducers is proportional to the normal surface velocity since these sensors have a dominant response to particle motion normal to the surface. Moreover, in Rayleigh wave-based reciprocity calibration, the sensor is mainly submitted to a normal vibration velocity because the fluid couplant strongly attenuates the in-plane component of the vibration [15]. A first approach to the calculation of the aperture function is provided by the ASTME [16], which consider that the sensor is hit by an ideal plane wavefront. Goujon & al. [17] refined the calculation of the aperture function by considering the case of a circular wavefront. In this paper, the size and shape of the sensor surface as well as the inhomogeneity of its sensitivity will be taken into account to estimate the output voltage. The influence of the size and shape of the sensor on the output voltage is given by the following integral:

$$U = \frac{1}{S} \iint_S \omega(r)\, m(r) dS \tag{1}$$

where:
U is the open circuit voltage across the receiving sensor,
S the active surface of the sensor,
ω is the normal velocity of a point of the sensor surface,
m is the sensitivity of a point placed at the distance r from the center of the sensor's surface.

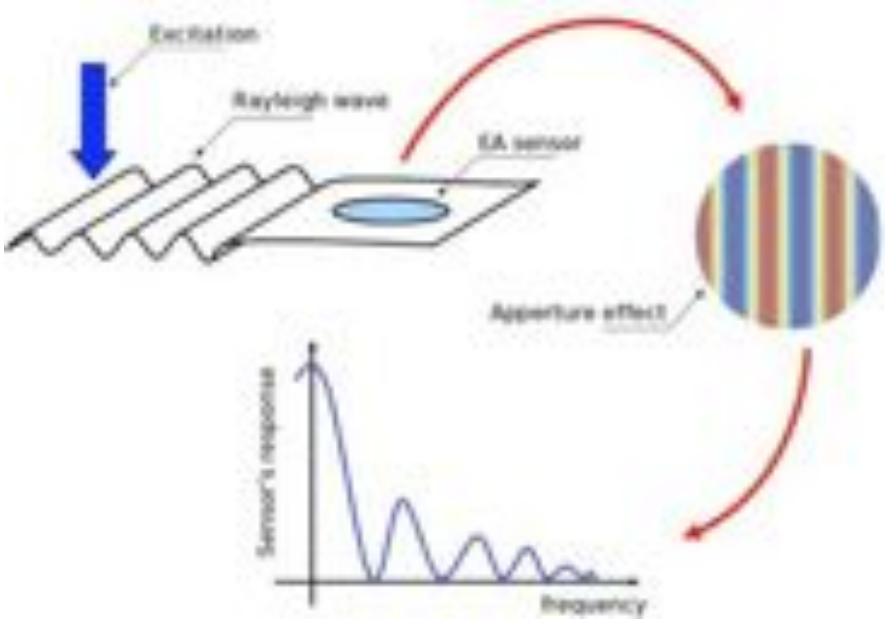

Figure 2: Illustration of the aperture effect

In the literature, a common assumption is to consider that $m(r)$ is uniform over the whole surface of the sensor. Consequently, in the case of cylindrical wave of amplitude A, the hypothesis $m(r) = m_0$ leads (1) to become:

$$U = \frac{m_0 A}{S} \iint_S \frac{e^{-jk_R r_0}}{\sqrt{r_0}} r dr d\theta \quad (2)$$

where r_0, r and D are defined in Figure 3, which picture the geometry used in the calculation of the aperture function.

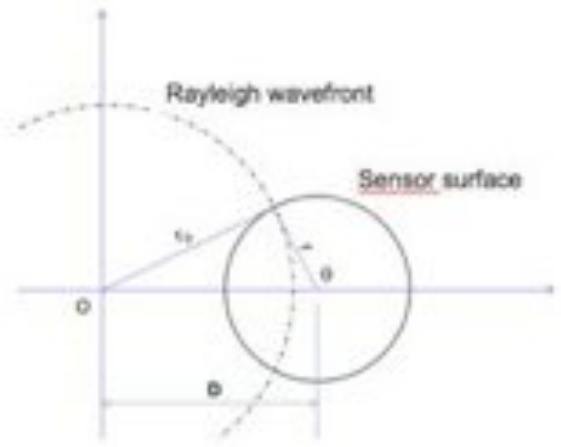

Figure 3: Geometry used in the calculation of the aperture function of the AE sensor

The receiving sensitivity of a sensor in Rayleigh waves M_R is defined as the ratio between the open circuit voltage of the sensor U and the normal component of the Rayleigh-wave velocity at the center of the sensor (r_0=D), which can be written as:

$$\omega(D) = \frac{A}{\sqrt{D}} e^{-jk_R D} \quad (3)$$

Then, the expression of M_R is:

$$M_R = \frac{m_0}{S}\sqrt{D}e^{jk_R D}\iint_S \frac{e^{-jk_R r_0}}{\sqrt{r_0}} r\mathrm{d}r\,\mathrm{d}\theta \tag{4}$$

With $k_R = 2\pi f/c_R$ the Rayleigh wavenumber, c_R being the velocity of Rayleigh wave in steel, it follows immediately:

$$M_R = m_0 F(f,S) = m_0 \frac{\sqrt{D}e^{jk_R D}}{S}\iint_S \frac{e^{-jk_R r_0}}{\sqrt{r_0}} r\mathrm{d}r\,\mathrm{d}\theta \tag{5}$$

which defines the aperture function *F* of the sensor.

The aperture function depends not only on the geometry of the sensor as well as on the frequency and geometry of the incident wavefront, but also on spatial variations of the sensitivity of sensor surface. Indeed, one can find in [17] mentions of experimental deviations between the experimental and theoretical aperture function, which could by attributable to the false assumption of uniform sensitivity m_0. Considering that the sensitivity of the sensor depends on the amplitude and phase of the free-end vibration of the sensor's surface. The new expression of the Rayleigh-wave sensitivity is thus:

$$M_R = \frac{\sqrt{D}e^{jk_R D}}{S}\iint_S m(r)\frac{e^{-jk_R r_0}}{\sqrt{r_0}} r\mathrm{d}r\,\mathrm{d}\theta \tag{6}$$

Here is made the assumption that the disc-shaped transducer exhibits an axisymmetric vibration profile, that is to say that *m(r)* is only function of the distance *r* from the center of the sensor's surface. Thus the complex expression of *m(r)* is:

$$m(r) = m_0\psi(r)e^{-j\varphi(\mathrm{r})} \tag{7}$$

where m_0 is the maximum sensitivity to normal vibration of the sensor surface and φ the phase shift of this vibration. $\psi(r)$ is a real number comprised between 0 and 1 so that the (5) holds with:

$$F(f,S) = \frac{\sqrt{D}e^{jk_R D}}{S}\iint_S \psi(r)\frac{e^{-j(\varphi(r)+k_R r_0)}}{\sqrt{r_0}} r\mathrm{d}r \tag{8}$$

In the next section we present the approach that has been used to experimentally determine $\psi(r)$ and $\varphi(\mathrm{r})$, which are subsequently used in the computation of the new aperture function $F(f,S)$.

3.1 Experimental setup

A laser scanning velocimeter was setup in order to determine the vibration profiles of the EA transducer as well as the vibration of the surface of a steel block used for Rayleigh-wave sensor calibration. These measurements will allow combining the actual sensor sensitivity with the theoretical diffraction effects due to the size of the transmitting and receiving areas, with regards to the wavelength of the Rayleigh waves.

As reminded in (1), the AE sensor voltage is the average of the normal velocity under its surface, weighted by its receiving sensitivity M_R defined in (4). M_R being referred to the Rayleigh wave vibration velocity at the center of the face of the sensor, it is independent from the amplitude *A* of the incoming wave. The sensitivity *m(r)* has the same dimension than M_R as seen in (6) and the aperture function *F* is dimensionless. In comparison with the definition

of (5), the dimensionless parameter $\psi(r)$ and $\varphi(\mathrm{r})$ are the only new parameters to be determined for the calculation of the new aperture function F defined in (8). Indeed, only the relative behavior of the sensor surface has to be determined in order to improve the representativeness of the aperture function since quantitative quantities such as the amplitude of the Rayleigh wave or the magnitude of the sensitivity m_0 do not appear in (8).

The laser interferometer detects the quasi-punctual normal velocity of the sensor, which is let to freely vibrate in air at atmospheric pressure. It is here assumed that the vibration behavior measured under free-boundary condition is representative enough of the one that could be expected when the transducer is coupled to the block with the fluid couplant. This question was addressed by measuring the vibration of the sensor when coupled to a glass block, which be more representative of the boundary conditions of the calibration method, but the laser measurement through the transparent block did not show a sufficient signal to noise ratio.

Thus, extrapolating the *relative* sensitivity of the sensor to be proportional to the experimentally determined normal velocity vibration profile allows recalculating the complex aperture function of the transducer with a non-uniform sensitivity *m(r)*.

3.1.1 Contactless measurement of the sensor's surface sensitivity

The acquisition of the velocity profile of the sensor surface was performed using a Polytec OFV 3001 laser velocimeter equipped with an OFV 303 head. The AE sensor used is a typical commercial PACμ80 sensor from Euro Physical Acoustics driven by an Agilent 33250A arbitrary waveform generator. For each point of the surface, the time signal is digitized by a Tektronix TDS3012B oscilloscope and stored in a personal computer for post processing (Figure 4).

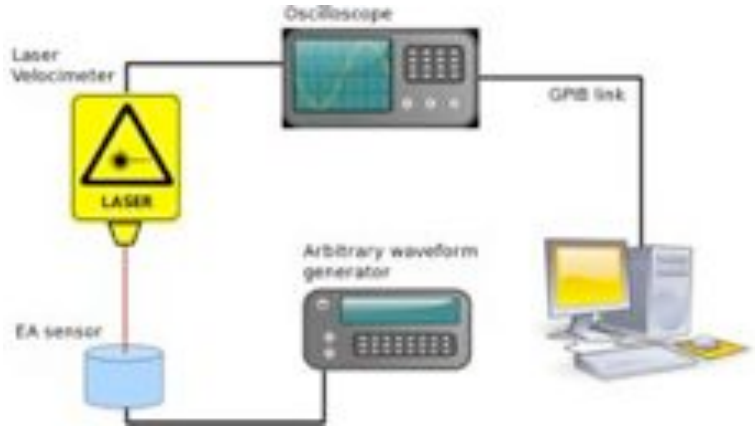

Figure 4: Measurement of the AE sensor normal velocity

The normal velocity of each point of the sensor surface is measured with a 100-μm spacing, when the electrical input is a sinusoidal excitation at 300 kHz. Figure 5a represents the peak-to-peak amplitude, in mm/s, of the velocity while Figure 5b represents its phase relative to the one measured at the center of the sensor. The dashed pink line pictures the outer circumference of the 9.5 mm diameter transducer. It can be seen that the local velocity at the sensor surface is far from being uniform, contrarily to the classical assumption of a piston-like behavior. The center area vibrates out-of-phase and with much higher velocity that the outer ring of the sensing surface. It has a diameter close to the 6.5 mm diameter of the piezoceramic, which is enclosed inside the transducer.

The magnitude and phase of the vibration of the surface being rather axisymmetric, it is decided to extract their profiles under this assumption, which meets the supposition made about the sensor being axisymmetric in (7).

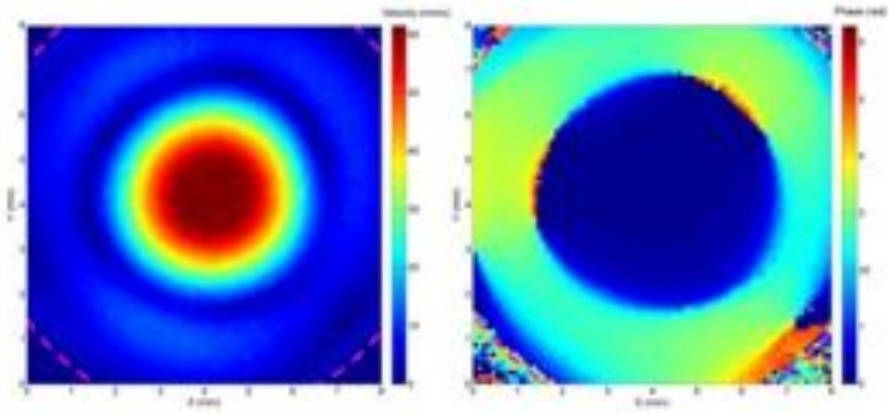

(a) (b)

Figure 5: Amplitude (a) and Phase (b) of normal velocity of the sensor's surface in free condition

Since the PACμ80 sensor is fairly resonant, the local sensitivity *m(r)* at the sensor face is derived from the local velocity measured at its central resonance frequency of 300 kHz. A proportionality relationship between those quantities is assumed. Figure 6, which pictures the modulus of the Fourier spectrum profiles extracted at various frequencies in the case of a pulsed excitation of the sensor, shows that the sensitivity profile of the sensor is also a function of frequency.

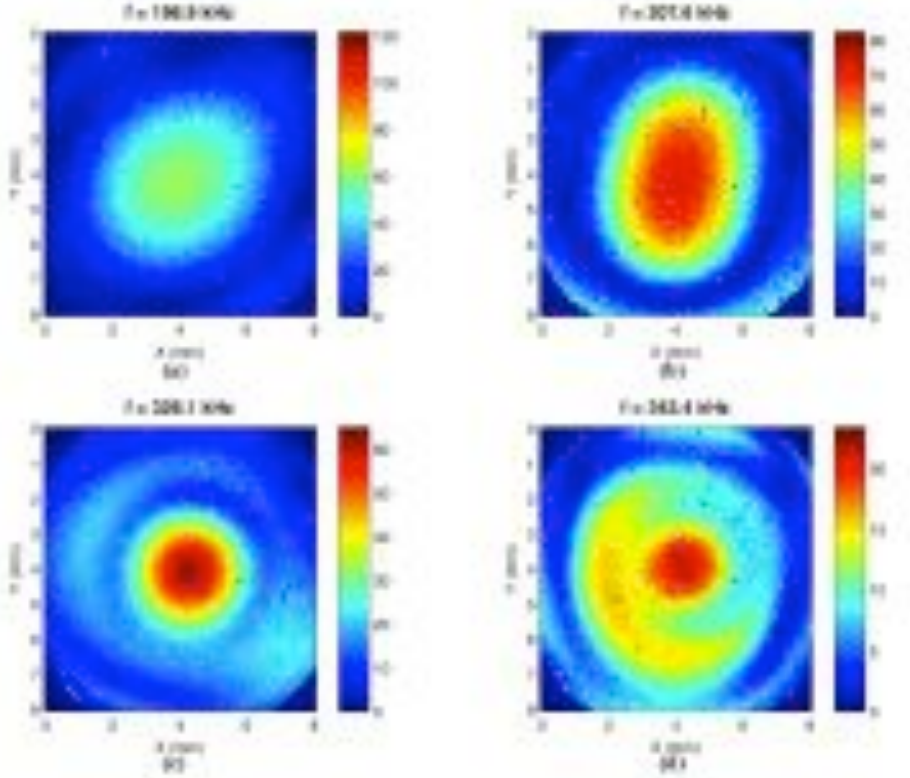

Figure 6: Amplitude profiles of normal velocity at various frequencies.

Consequently, the implementation of the proposed technique for a truly broadband sensor, which is quite rare in AE experiments, would require a procedure for extracting the complex sensitivity profile for each frequency component within the frequency band of the sensor.

In the present paper, it is decided to extrapolate the qualitative behavior of the sensor in the useful band as identical to the $\psi(r)$ and $\varphi(\mathrm{r})$ measured at 300kHz. Indeed, by virtue of the particularly resonant behaviour of this sensor, we assume that the qualitative effect of the difference between off-resonance velocity profiles is of the second order with regards to the quantitative effect of the variation of m_0 with the frequency, this later effect being actually taken into account.

3.1.2. Visualization of Rayleigh wavefront curvature in Rayleigh wave calibration

The Rayleigh wavefront that passes under the AE sensor is visualized using the same setup that the one described in [17], where a PACμ80 sensor, coupled with glycerin on a 300 × 300 × 400 mm steel transfer block, is used as an emitter and placed with its center at 30 mm from the center of the surface of interest. The transducer is driven with a short-pulse excitation provided by a Panametrics 5052 Pulser-Receiver. The interrogated surface has the same area that the one of Figure 5 and Figure 6 and is also scanned with a 100 µm spacing in both X and Y directions. Pictures of Figure 8 taken at close instants show that the wavefront propagating from left to right has a low curvature despite the relatively small distance between the transmitter and the reception area. This helps to understand the weak influence of the calculation proposed in [17] compared to the classical calculation involving a plane wavefront [16], as it will be shown in the next paragraph.

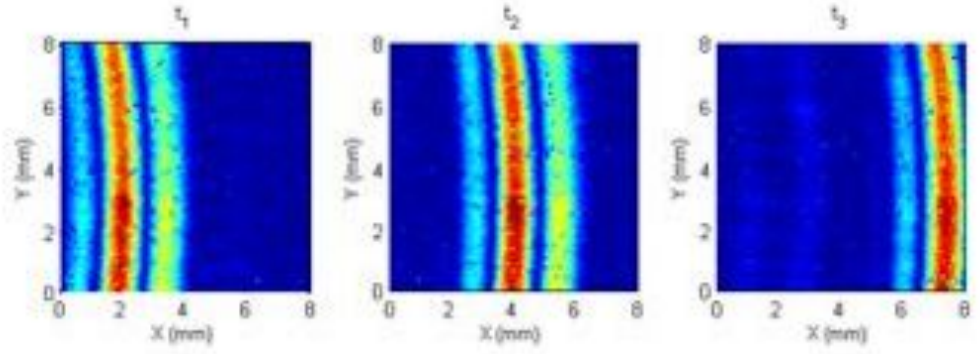

Figure 7: Snapshots at consecutive instants showing the curvature of the wavefront

3.2 Application towards a better consideration of the actual aperture of AE sensor

Figure 8 gathers, in the 1 MHz frequency range, the results in terms of aperture function obtained for the two referenced models and for the present model, where the information of amplitude of vibration was first only added, then complemented by the information of phase. The solid line in Figure 8 represents the aperture function proposed by the ASTM model [16] of a 300kHz plane Rayleigh waves on stainless steel, by taking into account the actual active area of the sensor of about 6.5 mm in diameter instead of the 9.5 mm diameter of the sensor's sole. This function behaves like a squared cardinal sine, and exhibits one null value within the measured frequency range of 1MHz, which is the upper frequency commonly used for the calibration of such kind of AE sensors. The dashed line in Figure 8 represents the aperture function obtained by Goujon & al. model when the radius of curvature of the Rayleigh-wave beam from a remote transmitter is also taken into account. It is almost the same as the solid one because the wavefront of the cylindrical wave is here relatively flat, as one can observe in Figure 7. So, the incoming wave from the actuator placed at a distance of 30 mm is quite close to the plane wave considered in the ASTM model.

Taking into account the actual amplitude of vibration velocity sensor, the first cut-off frequency of the aperture function occurs at about 1.05 MHz. Moreover, if one also reflects the phase shift of vibrations of the surface, still under the assumption of axial symmetry, the widening of the first lobe of the aperture function is slightly less than when accounting for the amplitude only. Knowing the difficulty to accurately measure the phase, it can be suggested that only considering the amplitude information may be sufficient to partially correct the aperture function without significant practical difficulty.

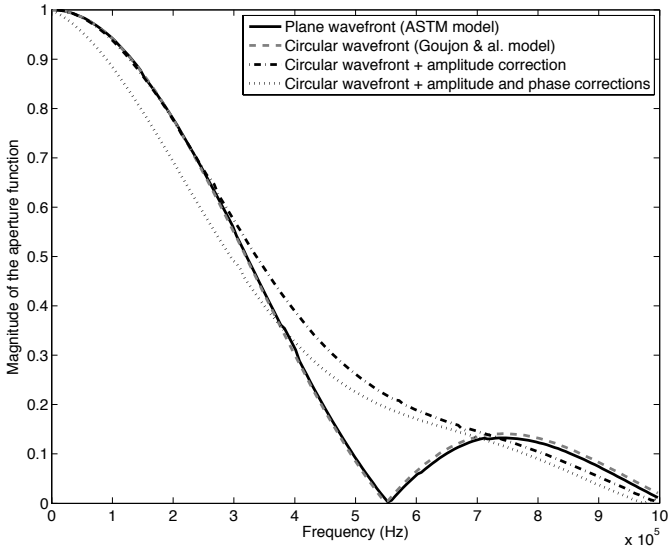

Figure 8: Aperture function in the 0 to 1MHz frequency range

Aiming at performing a calibration of acoustic emission sensors on the surface of a block transfer (Rayleigh-wave calibration) instead of using the usual bulk-wave calibration method requires taking into account the aperture effect of the sensor.

In order to check the validity of the aperture effect correction in surface wave calibration, the PACμ80 sensor sensitivity to Rayleigh waves is compared to the one obtained with longitudinal bulk waves. To produce the incident bulk wave, a longitudinal wave transducer was set to the opposite face of the block. The 300 mm thickness of the block is more than fifteen times the wavelength of longitudinal waves in steel and according to the relationship $d^2/(4\lambda)$=1.25 mm defining the near field limit of the sensor, the sensor is here in the far-field of the emitter. The radius of curvature of the wavefront travelling through the thickness of the propagating medium is large enough to consider it as a perfect plane wavefront. Since there is no aperture effect to be accounted for in the presence of such a plane wave of amplitude B hitting the sensor at normal incidence, the voltage across the sensor is:

$$U = \frac{B}{S}\iint_S m(r)\,dr\,d\theta = \frac{B}{S}\cdot m_0 \iint_S \psi(r)e^{-j\varphi(r)}\,dr\,d\theta \quad (9)$$

Under the hypotheses of the absence of geometrical influence of the frequency and axial symmetry of the *d* diameter sensor, (9) becomes:

$$U = m_0\frac{B}{S}2\pi\int_0^{d/2}\psi(r)e^{-j\varphi(r)}\,dr = m_0 BK(d) \quad (10)$$

with *K(d)* a constant value that is numerically computed. Hence the sensitivity to

longitudinal bulk wave M_L versus frequency shows a flat curve, which expression is:

$$M_L = m_0 K \tag{11}$$

Therefore, using (5) yields:

$$M_L = \frac{K}{F(f,S)} \cdot M_R \tag{12}$$

The aperture function $F(f,S)$ is the only quantity to be determined in order to validate the R-wave calibration method. The sensitivity to longitudinal bulk wave should thus be proportional to the ratio of the sensitivity to longitudinal bulk wave and the aperture function.

Figure 9 shows various sensitivity spectra of the sensor PACμ80. The curves represent the moduli of the complex sensitivities in the 1 MHz range. The solid curve shows the sensitivity obtained by bulk longitudinal-wave calibration whereas the dashed line represents the Rayleigh wave sensitivity, which we measured by applying the surface-wave reciprocity method proposed by Hatano [18]. According to (12), the bulk-wave sensitivity curve must be inferred from the Rayleigh-wave curve by simple division term by term.

In [17], Goujon *et al.* did not account for any geometrical variation of m, assuming $m=m_0$ e.g. $\psi(r)=1$ and $\varphi(r)=0$, yielding $K=1$. The dashed-dotted curve with cross markers is obtained according to the piston-like behavior model, which considers a uniform and in-phase displacement of every point of the surface of the sensor, e.g. considering $K = 1$ and substituting in (12) the aperture function F given by (5). The sensitivity curve thus obtained clearly not fit the sensitivity measured with bulk longitudinal waves, what invalidates the Goujon & al. model. Without detracting from the quality of the work of these authors, say that their assumptions prevent to correctly account for the aperture effect outside the low frequency range. Indeed, the too fast decay of the aperture function depicted in Figure 8 makes the recalculated curve deviate from the experimental curve when the frequency exceeds about 400 kHz. In addition, the vanishing of the denominator for the cut-off frequency at f = 550kHz causes the divergence of the recalculated M_L sensitivity. We believe that the presentation in [17] of results only for frequencies below this first cut-off frequency, combined with the fact that the approach was to calculate the sensitivity of Rayleigh waves from the sensitivity of bulk waves by multiplying the aperture function, thus avoiding the above mentioned problem of divergence, has overshadowed the limitations of the piston–like model.

The curve with black dot markers in Figure 9 pictures the bulk-wave sensitivity spectra obtained from the Rayleigh-wave sensitivity spectra divided by the new aperture function model (8). It shows a good agreement with the experimental curve for frequencies up to 450kHz and a reasonable agreement for frequency above this value. As no normalization of the measured bulk-wave or Rayleigh-wave sensitivities were performed, on can deduce that the value of $K(d)$ is here close to 1. The good fit between the experimental curves and those derived through our aperture function, itself based on precise measurements of the vibrational behavior of the sensor, confirms our approach and validates the proposed model.

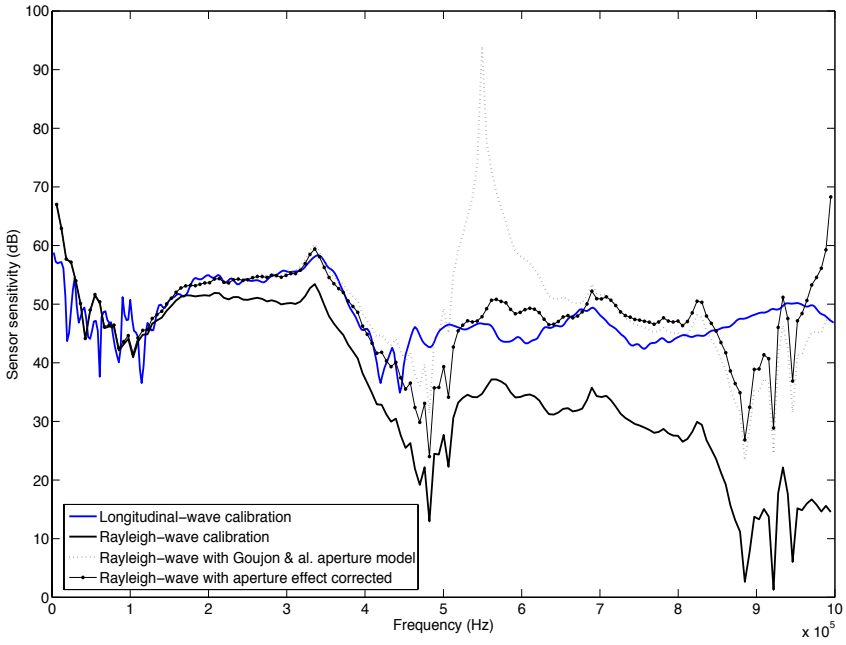

Figure 9: Aperture effect correction of R-wave sensitivity and comparison with L-wave sensitivity in the 1MHz range

In the previous section we mentioned that aperture effect undermines the reciprocity criterion. With the new aperture function, we showed that L-wave sensitivity can be derived from R-wave sensitivity. In other words R-wave configuration for AE sensor meets reciprocity criterion.

4. Shear wave calibration of AE sensors

To our knowledge there are no previous attempts of S-wave calibration of AE sensors. Our first attempt was the classic arrangement for reciprocity calibration: three AE sensors and a propagating medium. The experimental arrangement is the same as the one Hatano used for L-wave calibration of AE sensors in [18]. With that method, it is possible to detect S-wave but it is not possible to isolate it from the whole signal. Indeed S-wave is partly buried in the preceding L-wave. To workaround that issue, normal incidence S-wave transducers (*Panametrics V151)* have replaced two of the AE sensors. As S-wave calibration requires repeatable sensor coupling, a solid cement was used to validate the method. For practical reasons, namely to ease the sensor repositioning, a thick couplant was also used. This shear wave couplant from *Sofranel* showed good repeatability and produced comparable result to the one that was get from the use of the cement.

As shown in Figure 10 the L-wave component became negligible compared to S-wave. Before computations the L-wave component is removed by proper windowing.

Conventional hardware has been used for the calibration. Current is sent to the emitting sensor by means of the *Agilent 33210A* arbitrary waveform generator. *Philips PM9355* current probe/amplifier is used to measure current absorbed by the emitting sensor. A *Bruel & Kjaer 2638* amplifier is used to preamplify the voltage across the receiving transducer. Finally, a Tektronix Tds-340 oscilloscope records voltages with 512 averages.

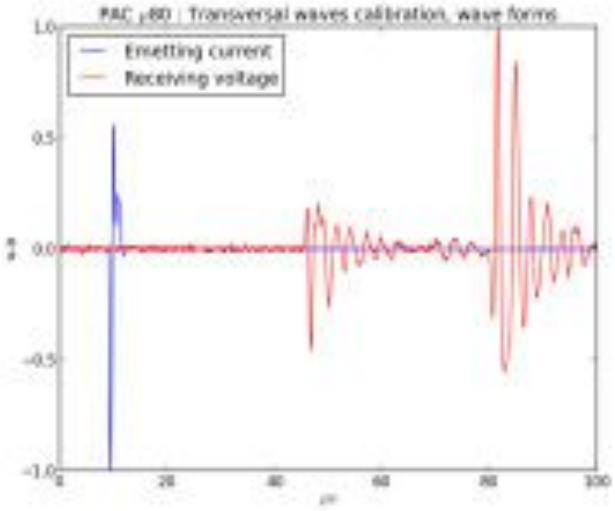

Figure 10: current absorbed by the emitter and voltage across the AE sensor in S-wave calibration

What can be observed in Figure 11 is the comparison between L-wave and S-wave sensitivities. It appears that the S-wave sensitivity is 15 dB below L-wave sensitivity. However both sensitivities have the same evolution.

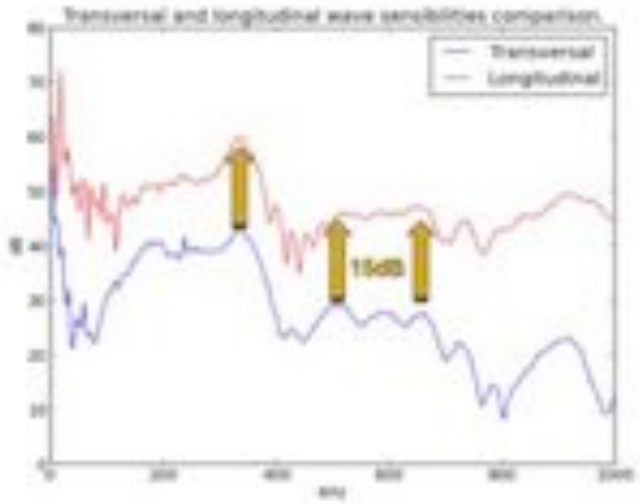

Figure 11: S-wave calibration of a PACµ80 sensor: comparison with L-wave sensitivity

Tests conducted with other sensors, for instance with a PAC R-15alpha sensor (), and different coupling fluids confirmed this trend.

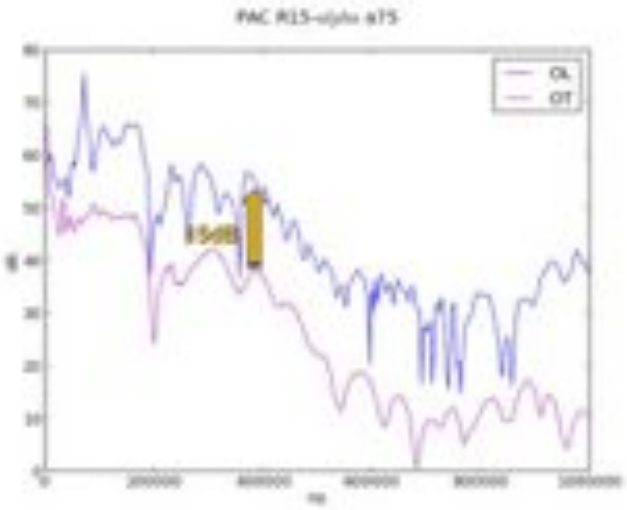

Figure 12: S-wave calibration of a PACμ80 sensor: comparison with L-wave sensitivity

S-wave AE calibration is a prime. We proposed a method with one AE sensor and two normal incidence S-wave transducer. Obtained results have demonstrated the technical feasibility of that method. It is also important to note that S-wave sensitivity and L-wave sensitivity are linked. As a result, relying on R-wave sensitivity and the aperture function, one can derive L-wave sensitivity and finally S-wave sensitivity.

5. Conclusion

Although proper definition of the reciprocity parameter is not a simple task, the objective of this paper was to present elements that are essential to a better understanding of the reciprocity parameter. First we have seen that Bobber's conclusions give physical insight to the definition of this parameter and that Hill and Adams extended it to AE sensors calibration. Next we presented a new aperture function. We have seen that aperture effect correction of R-wave sensitivity can be used to derive L-wave sensitivity. Finally, an original method for S-wave calibration of AE sensors has been presented. The first results showed that it might be possible to derive S-wave sensitivity from L-wave sensitivity. As a result it can be infer that knowledge of R-wave sensitivity is sufficient for the complete characterization of AE sensors.

Acknowledgements
This work was conducted as part of the MACSIM project, dealing with modeling of acoustic emission testing and funded by the French National Research Agency. The project partners are CEA LIST, CETIM, DCNS, EADS IW, and EXTEND UTC

References

1 Bleaney, B. I., Bleaney, B., Electricity and magnetism, 2nd édition. Oxford University Press, Oxford [1965].
2 McLean, W. R., Absolute measurement of sound without a primary standard. J. Acoust. Soc. Amer. **12** [1940], 140.
3 Breckenridge, F. R., Watanabe T., Hatano H., Calibration of acoustic emission transducers: comparison of two methods. Progress in Acoustic Emission, Vol. **1**, [1982], 448-458.
4 Hatano H., Mori E., Acoustic-emission transducer and its absolute calibration, J. Acoust. Soc. Amer. **59** [1976], 344.

5 Hill, R., Adams N. L., Reinterpretation of the reciprocity theorem for the calibration of acoustic emission transducers operating on a solid. Acoustica **43** [1979], 305-312.
6 Hatano H., Chaya T., Watanabe S., Jinbo K., Reciprocity Calibration of Impulse Responses of Acoustic Emission Transducers, IEEE Transactions on ultrasonics, ferroelectrics and frequency control, Vol. **45** (5) [1998], 1221-1228.
7 Keprt J., Benes P., Determination of Uncertainty in Calibration of Acoustic Emission Sensors, Hellenic Society for NDT, [2007], Chania, Crete-Greece
8 Keprt J., Benes P., Progress in Primary Calibration of Acoustic Emission Sensors, Acoustic [2008], Paris, 2217-2222.
9 Keprt J., Benes P., Primary calibration of acoustic emission sensors, Fundamental and Applied Metrology, [2009], Lisbon, Portugal
10 Bobber, R. J., General reciprocity parameter. J. Acoust. Soc. Amer. **39** [1966], 680.
11 Lamb H., On the propagation of tremors over the surface of an elastic solid., Philos. Trans. A203 [1904], 1.
12 Hill R., Reciprocity and other Acoustic Emission Transducer Calibration Techniques, J. Acoustic Emission **1** [1982], 73-80.
13 Gorman M.R., Ziola S. M., Plate waves produced by transverse matrix cracking, Ultrasonics **29** [1991] 251.
14 Gorman M.R., Plate Wave Acoustic Emission, J. Acoust. Soc. Amer. **90** [1991] 358-364.
15 Theobald P., Zeqiri B., Avison J. Couplants and their influence on AE sensor sensitivity, J. Acoustic Emission [2008] 26
16 ASTM Non destructive Testing Handbook: Acoustic Emission Testing 2nd ed. (Columbus, OH: American Society for Non Destructive Testing) [1987] 126-30
17 Goujon L., Baboux J. C., Behaviour of acoustic emission sensors using broadband calibration techniques, Meas. Sci. Technol. **14** [2003] 903-908.
18 Hatano, H. and Watanabe, T., Reciprocity Calibration of Acoustic Emission Transducers in Rayleigh-Wave and Longitudinal-Wave Sound Fields, J. Acoust. Soc. Am., Vol. **101** [1997], 1450-1455.